Influence of film-thickness on the ozone detection of perovskite La0.8Pb0.1Ca0.1Fe1–xCoxO3 based sensors

S Smiy, M Bejar, E Dhahri, T Fiorido, K Aguir, V. Laithier, M Bendahan

Film-thickness influence on ozone detection of perovskite $La_{0.8}Pb_{0.1}Ca_{0.1}Fe_{1-x}Co_xO_3$ based sensors

S. Smiy [a], M. Bejar [a,*], E. Dhahri [a], T. Fiorido [b], K. Aguir [b], V. Martini-Laithier [b], M. Bendahan [b]

[a] *Laboratoire de Physique Appliquée, Faculté des Sciences, B.P. 1171, 3000 Sfax, Université de Sfax, Tunisie.*

[b] *Aix Marseille Univ, Université de Toulon, CNRS, IM2NP, Marseille, France*

Abstract

In this study, $La_{0.8}Pb_{0.1}Ca_{0.1}Fe_{1-x}Co_xO_3$ (x = 0.10 and x = 0.20) thin films with respective thicknesses of 300 and 600 nm have been prepared by the drop coating technique onto Si/SiO_2 substrate with platinum interdigitated electrodes. The effect of cobalt-content and films thickness on the ozone sensing properties have been studied. The sensors responses have been determined in an operating temperature range between 160 and 280°C. Sensors have been exposed to different concentrations between 50 and 400 ppb of ozone gas at a constant flow rate of 500 ml/min dry air.

The studied $La_{0.8}Pb_{0.1}Ca_{0.1}Fe_{1-x}Co_xO_3$ (x = 0.10 and x = 0.20) compounds could be a promising sensitive film for ozone detection, especially for the thinnest sensitive layer, 300 nm in our case.

***Keywords*:** Perovskite, Sensors, Thin films, Films thickness, Ozone sensor.

Corresponding author: bejar_moez@yahoo.fr (**M. Bejar**)

I- INTRODUCTION

Ozone (O_3) is an oxidizing gas, which is used in various fields such as food, odor control and medical disinfection **[1]**. However, above a concentration of 90 ppb, ozone gas leads to health problems and become very harmful above a concentration of 160 ppb **[2]**. The **W**orld **H**ealth **O**rganization (WHO) declared that the 8 h average ozone gas exposure limit is 75 ppb **[3]**. Hence, many materials have been recently investigated as ozone-gas based sensors. Among them, metal oxide semiconductors are widely used such as ZnO **[4, 5]**, WO_3 **[6,7]**, SnO_2 **[8]** and In_2O_3 **[9]** added to that we have other materials which are used for gas sensing applications **[10-13]**. Though, the complicated fabrication processes are

still the main drawback of these materials. These materials are currently studied in forms of nanostructured such as nanowires, nanotubes and nanorods thanks to their large surface area and nano-size effect **[14,15]**. But these materials are characterized by a very high operating temperature for example in the case of WO_3 and Au-ZnO prepared by the hydrothermal method, the operating temperature is found to be equal to 200°C and 206°C, respectively, in presence of 1000 ppb of BTEX **[16]**. Added to that, many works are interested on the study of materials which are nonporous, mesoporous and other materials characterized by nanometric size used for gas sensing application **[16-18]**.

Perovskite materials are promising candidates for the detection of ozone-gas **[19-23]**. For instance, $SrTi_{0.85}Fe_{0.15}O_3$ sensor was used in the detection of 800 ppb of ozone gas at the operating temperature of 250 °C **[22]**. M. Mori et *al*. found that introducing Co **[24]** in place of Fe was accompanied by a decrease in the operating temperature of this sensor **[23]**. $LaFeO_3$ is a multifunctional perovskite material, which was used in the detection of many dangerous oxidizing gases such us NO_2 **[25]** and SO_2**[26]**.

However, $LaFeO_3$ is characterized by a high resistance **[27]**, which is a disadvantage in the field of gas sensors. For this reason, it is necessary to replace the lanthanum in $LaFeO_3$ with lower-valence cations, such as Sr, Ca and Pb **[28-30].** The gas-sensing properties of $La_{1-x}Ca_xFeO_3$ and $La_{1-x}Pb_xFeO_3$ have been studied respectively by L.B. Kong et ***al.*** **[31]** and P. Song et ***al.*** **[32]**. It has been confirmed that these perovskites, with a composition where $x = 0.2$, show a higher response and greater selectivity to CO and ethanol gases, respectively. Usually, the perovskite materials used in the field of gas sensing are used in pellets forms, therefore and in order to increase the sensitivity of these sensors it is necessary to deposit these materials using chemical method which is sol gel by drop coating because the response increases in case of the use of chemical preparation method **[33].**

In our previous published work related to this framework, we have demonstrated that introducing cobalt instead of Iron in $La_{0.885}Pb_{0.005}Ca_{0.11}Fe_{1-x}Co_xO_{2.95}$ ($x = 0.00, 0.05, 0.10\ and\ 0.15$) compounds leads to the decrease of the operating temperature from 270 °C to 250 °C when Co-content increase from 0 % to 5 % in presence of the NH_3 reducing gas **[29]**. Moreover, the responses of $La_{0.8}Pb_{0.1}Ca_{0.1}Fe_{1-x}Co_xO_3$ ($0.00 \leq x \leq 0.20$) sensors found in this study were higher than those of $La_{0.885}Pb_{0.005}Ca_{0.11}Fe_{1-x}Co_xO_{2.95}$ ($0.00 \leq x \leq 0.15$) sensors found in our previously

study **[29]**. But in these works, perovskite materials are used in pellets forms. In this context, in our recent article, the substitution of Fe by Co and substitute La by Ca and Pb in $LaFeO_3$ sensor can lead to an increase of the response S and a decrease of the operating temperature for these materials **[28-34].** The aim of the present work was to develop $La_{0.8}Pb_{0.1}Ca_{0.1}Fe_{1-x}Co_xO_3$ films ($x = 0.10$ and $x = 0.20$) by drop-coating method based on the use of nano-powders synthesized by the sol-gel technic. Also, in this work, the O_3 sensing properties of our sensors as a function of films thickness are investigated.

II- EXPERIMENTAL DETAILS

II-1) Elaboration of nano-powders and thin films deposition

A series of $La_{0.8}Pb_{0.1}Ca_{0.1}Fe_{1-x}Co_xO_3$ (x = 0.10 and x = 0.20) samples have been prepared using the sol-gel technic with $La(NO_3)_3 6H_2O$, $Pb(NO_3)_2 2H_2O$, $Ca(NO_3)_2 6H_2O$, $Fe(NO_3)9H_2O$ and $Co(NO_3)_2 6H_2O$ as precursors (all chemicals were of 99.99% purity and purchased from Sigma-Aldrich). Firstly, precursors have been dissolved in distilled water to obtain a mixed solution. Citric acid $C_6H_8O_7$ and few drops of ethylene glycol have been added when these nitrates are completely dissolved in order to ensure homogenization and gel formation (the ratio amount of citric acid/ethylene glycol was 1:4). The obtained powders are sintered respectively at 300 °C (24 h), 600 °C (24 h) and 900 °C (24 h) to obtain the corresponding phase. Finally, the structure of the prepared compounds has been characterized by X-ray diffraction using CuK_α radiation $(\lambda = 1.5406\ \text{Å})$. The thin films deposition of the prepared compounds has been performed on Si/SiO_2 substrate by the drop-coating technique. A mixture of 20 mg and 20 ml of 2-propanol has been prepared for each compound. The suspensions have been ultrasonicated for 10 min at 40 °C in order to ensure homogenization for the mixture. The coating of Si/SiO_2 substrate with inter-digitated Pt-electrodes, has been carried out drop by drop using a micropipette. Two thin films have been obtained after the deposition of 8 and 16 drops which correspond to 20 µl and 40 µl, respectively. The deposition of thin films was followed by an annealing for 1 h at 500 °C.

II-2) Gas sensitivity measurements

We investigated the O_3 sensing properties of our $La_{0.8}Pb_{0.1}Ca_{0.1}Fe_{1-x}Co_xO_3$ material for two film thicknesses 300 nm (8 drops) and 600 nm (16 drops) for x = 0.00 and x = 0.20. Sensors

have been placed in a test chamber which allowed the control of the temperature under variable O_3 concentrations (***Figure 1***).

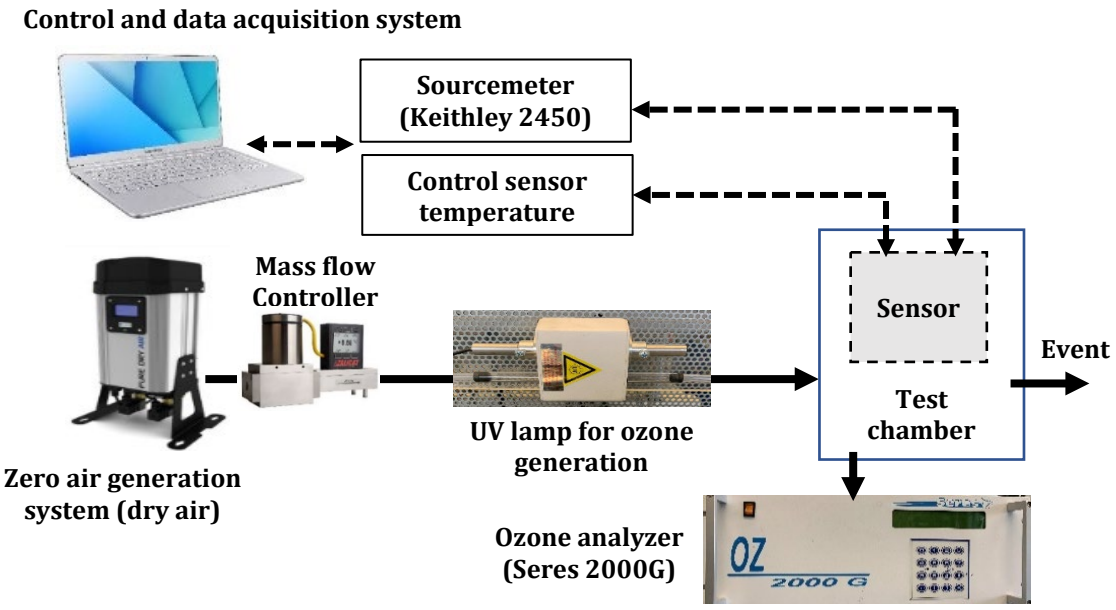

Figure 1: General diagram of measurements setup used to characterize ozone microsensors.

The volume of the chamber is about 2 liters. Dry air has been used as a reference gas. Ozone gas has been generated by oxidizing a part of oxygen in the dry air using a pen-ray UV lamp (Stable Ozone Generator UVP/185 nm). The different ozone concentrations have been obtained by partially masking the UV lamp whose range is between 30 ppb and 800 ppb with a dry air flow rate maintained at 0.5 ℓ / min. An ozone analyzer (reference Seres 2000G), has been used to calibrate and verify the correct ozone concentrations during the tests. The operating temperature of $La_{0.8}Pb_{0.1}Ca_{0.1}Fe_{1-x}Co_xO_3$ based sensors has been adjusted between 160 °C and 280 °C in order to optimize the sensor response. The sensor bias voltage has been fixed to 1 V and the current is measured using a keithley 4250 sourcemeter. The response S is defined as:

$$S = \frac{R_a}{R_g} \qquad (\boldsymbol{Eq.1})$$

Where R_a is the sensor resistance under dry air and R_g the sensor resistance under ozone with dry air.

III- RESULTS AND DISCUSSION

III-1) *XRD* and *EDX* studies

In order to check the crystallinity of $La_{0.8}Pb_{0.1}Ca_{0.1}Fe_{1-x}Co_xO_3$ (x = 0.10 and x = 0.20) nanopowders, a Bragg (θ-2θ) *X*-ray diffraction (*XRD*) has been applied, CuKα radiation ($\lambda = 1.5406$ Å) and 0.02 angle step have been used for the *XRD* analysis. The analysis of *XRD* patterns (***Figure 2***) proves that the prepared samples crystalize in the orthorhombic system with *Pnma* group **[19]**.

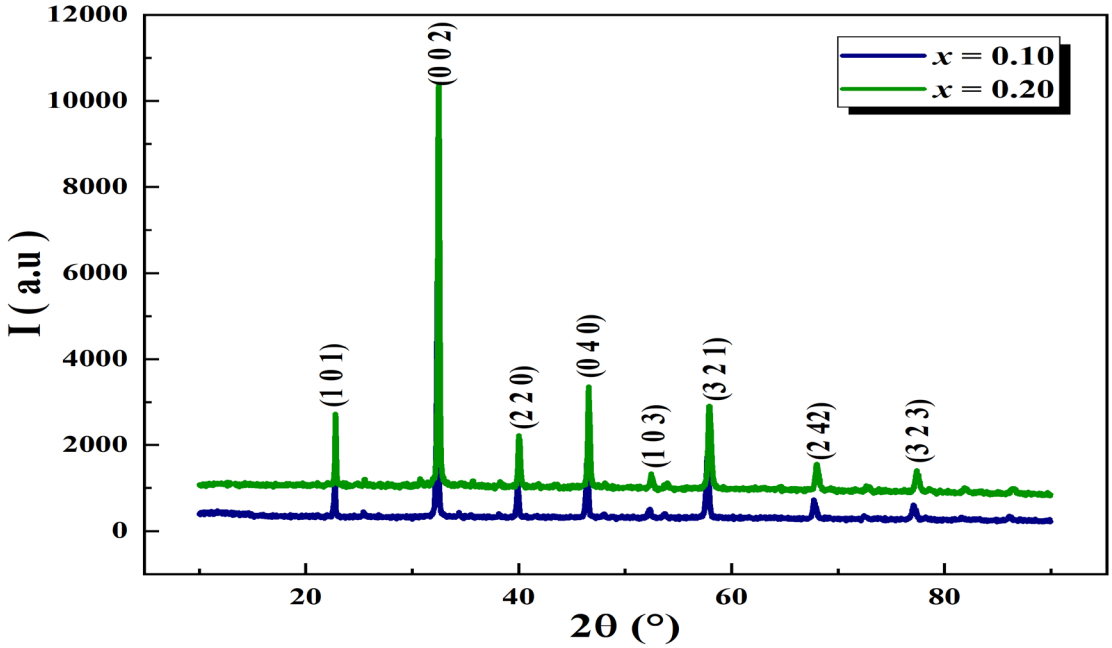

Figure 2: X-ray diffraction patterns of $La_{0.8}Pb_{0.1}Ca_{0.1}Fe_{1-x}Co_xO_3$ (x = 0.10 and x = 0.20) compounds, all peaks are indexed in the orthorhombic *Pnma* symmetry.

The (*hkl*) Miller indices of the most intense peaks are (101), (002), (220), (040), (103), (321), (242) and (323). The energy dispersive spectra (*EDX*) and SEM graphs of $La_{0.8}Pb_{0.1}Ca_{0.1}Fe_{1-x}Co_xO_3$ (x = 0.10 and x = 0.20) sensors are depicted in ***Figures 3*** (a, b) and ***Figures 3*** (c, d) the results reveal the presence of the characteristic peaks of La, Pb, Ca, Fe and Co elements.

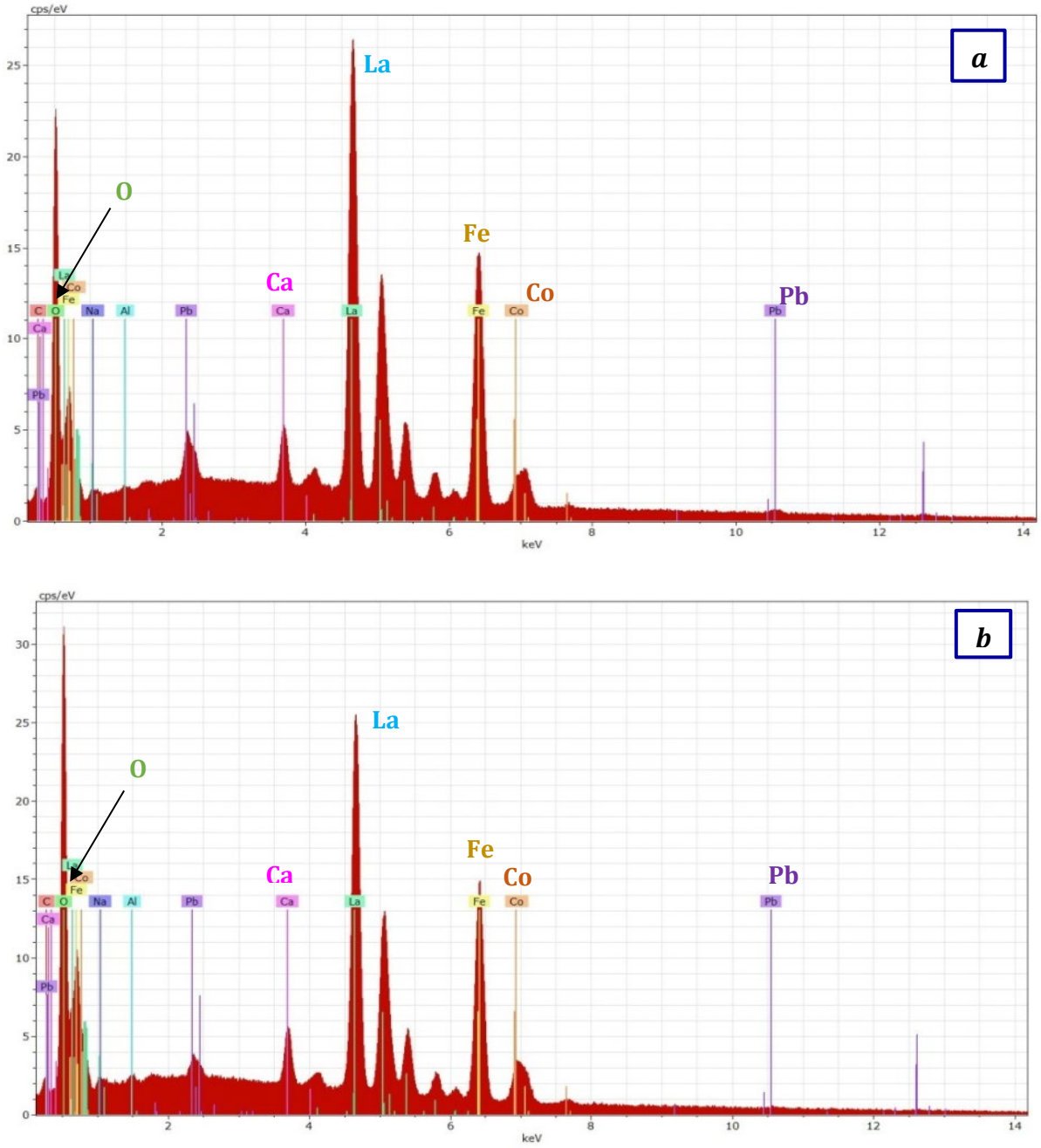

Figure 3 (*a*, *b*): Energy dispersive spectra (EDX) of $La_{0.8}Pb_{0.1}Ca_{0.1}Fe_{1-x}Co_xO_3$ (x = 0.10 **(a)** and x = 0.20 **(b)**) sensors.

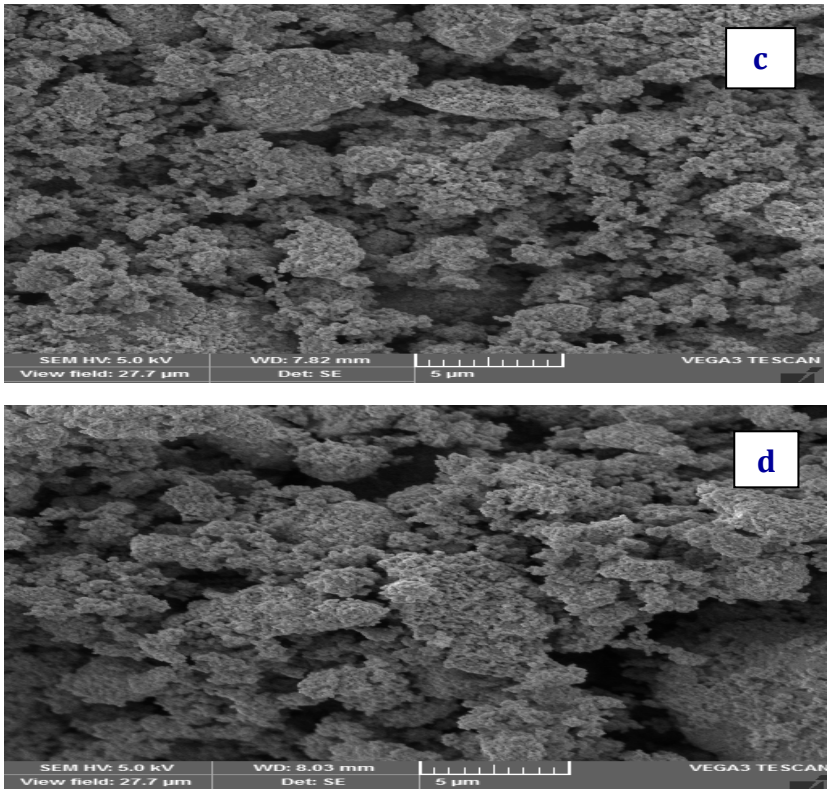

Figure 3 (*c*, *d*): SEM-graphs of $La_{0.8}Pb_{0.1}Ca_{0.1}Fe_{1-x}Co_xO_3$ (x = 0.10 **(c)** and x = 0.20 **(d)**) sensors.

The grain size was determined by using the Scherrer method **[35]:**

$$D_{SC} = \frac{k \times \lambda}{\beta \cos \theta} \qquad (\boldsymbol{Eq.2})$$

Where k is the grain form factor ($k = 0.9$), $\lambda = 1.5406$ Å represents the wavelength, θ defines the Bragg angle for the most intense peak and β is the full width at half maximum of the most intense peak.

The calculated value of the crystallite size (D_{SC}) was found equal to 43.4 nm and 43.2 nm for $x = 0.10$ and $x = 0.20$, respectively. The obtained values are comparable to those found for other compounds considered as nanometric materials for gas-sensing application **[36, 37]**. Moreover, it is reported that nanometric materials present significant activity and consequently, facilitate the chemisorption of oxygen of these compounds **[38]**. Finally, it is worth to mention that the incorporation of the Co ion in place of Iron leads to the decrease of the crystallite size value.

III-2) Dependence between film thickness and ozone sensing properties of $La_{0.8}Pb_{0.1}Ca_{0.1}Fe_{1-x}Co_xO_3$ ($x = 0.10, x = 0.20$) sensors

The deposition of $La_{0.8}Pb_{0.1}Ca_{0.1}Fe_{1-x}Co_xO_3$ ($x = 0.10$ and $x = 0.20$) nano powders over the Si/SiO_2 substrate has been checked by optical microscope analysis. The results depicted in ***Figure. 4***, show the optical views of $La_{0.8}Pb_{0.1}Ca_{0.1}Fe_{1-x}Co_xO_3$ (x = 0.10 and x = 0.20) compounds after deposition of 8 and 16 drops.

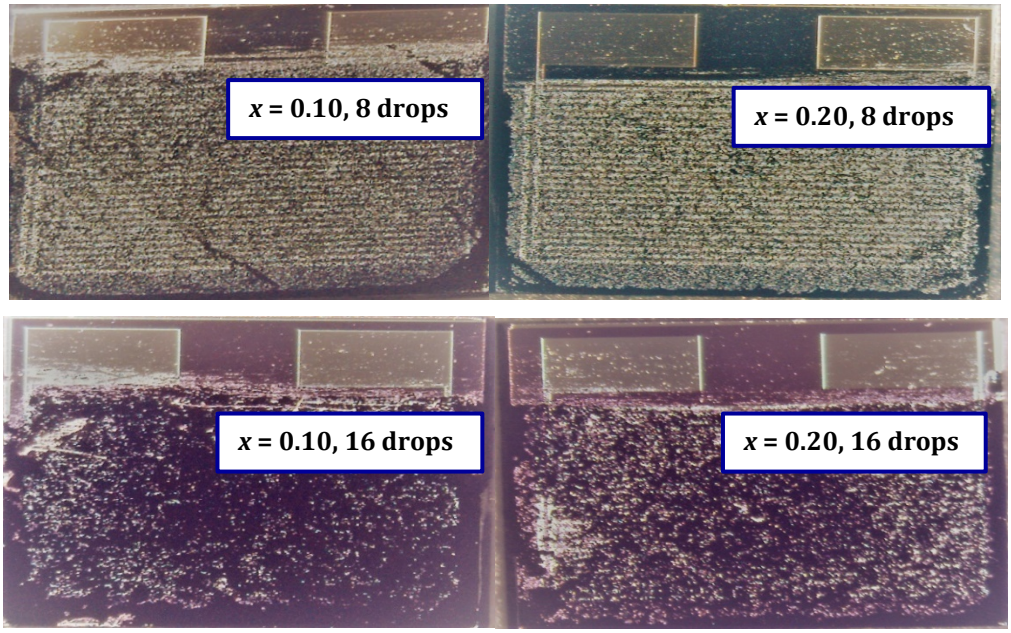

Figure 4: Optical view of $La_{0.8}Pb_{0.1}Ca_{0.1}Fe_{1-x}Co_xO_3$ (x = 0.10 and x = 0.20) sensors after deposit of 8 and 16 drops.

Film's thickness has been measured after annealing using a DEKTAK 6M mechanical profilometer. The average film thickness was found to be equal to 300 nm and 600nm for coating process with 8 and 16 drops, respectively (***Table 1***).

Table 1: Mean thickness, standard deviation, and repeatability error of $La_{0.8}Pb_{0.1}Ca_{0.1}Fe_{1-x}Co_xO_3$ (x = 0.10 and x = 0.20) sensors.

	Thickness (nm)						Mean thickness (nm)	Standard deviation (nm)	Error repeatability (%) = (Standard deviation/Mean thickness)
	test 1	test 2	test 3	test 4	test 5	test 6			
8 drops	288	316	321	302	287	286	300	15,5	5
16 drops	589	604	609	612	599	588	600	10	1,7

After the deposit of our material, measurements of the sensor resistance as a function of time have been carried out at different temperatures and with different $La_{0.8}Pb_{0.1}Ca_{0.1}Fe_{1-x}Co_xO_3$ (x = 0.10 and x = 0.20) film thicknesses (***Figures 5*** and ***6***).

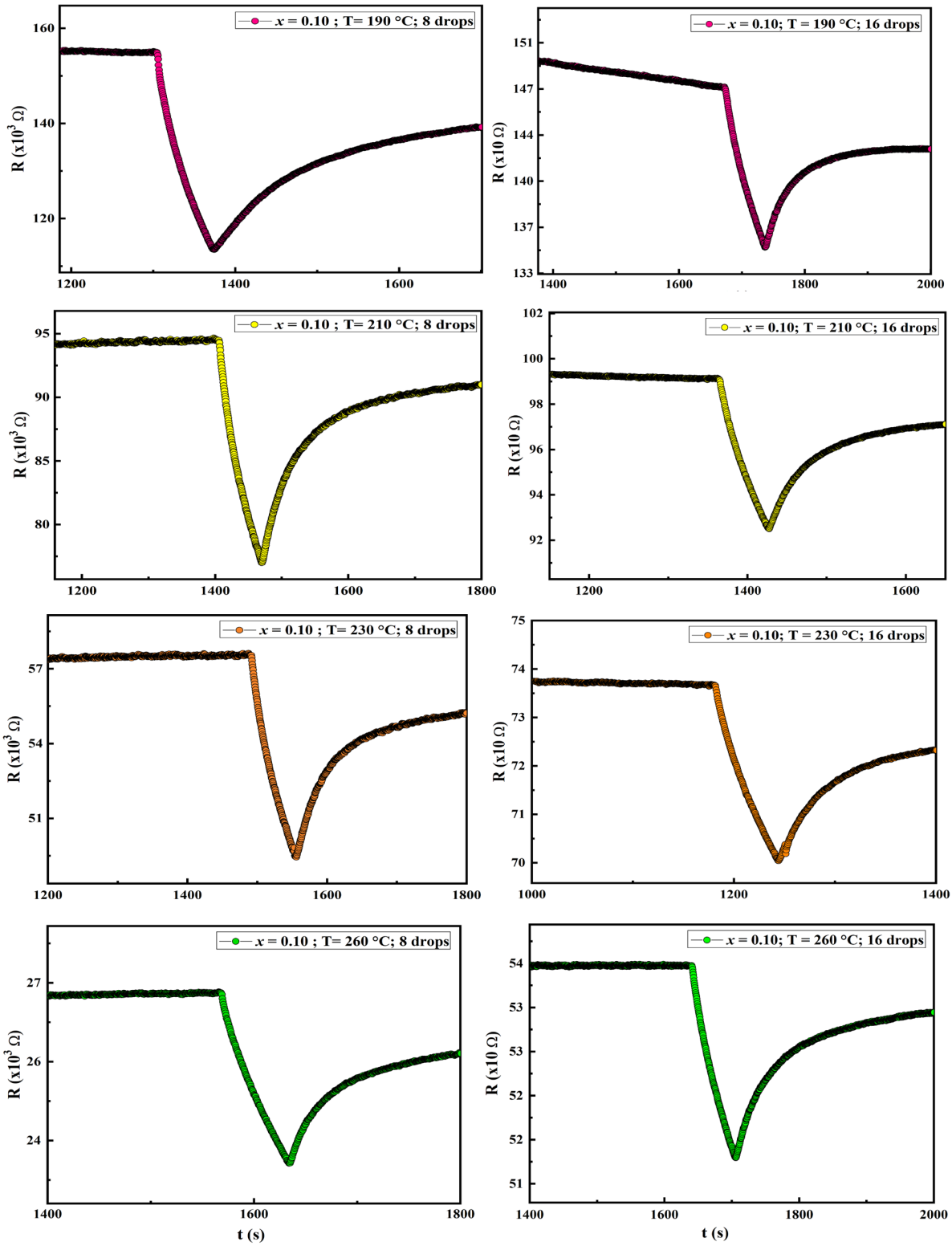

Figure 5: Ozone gas response of $La_{0.8}Pb_{0.1}Ca_{0.1}Fe_{0.9}Co_{0.1}O_3$ ($x = 0.10$) sensor as a function of time at several temperatures (190, 210, 230 and 260 °C) for a thickness film equal to 300 nm (8 drops) and 600 nm (16 drops) for an exposure time equal to 1 min ($\boldsymbol{C = 100\ ppb}$).

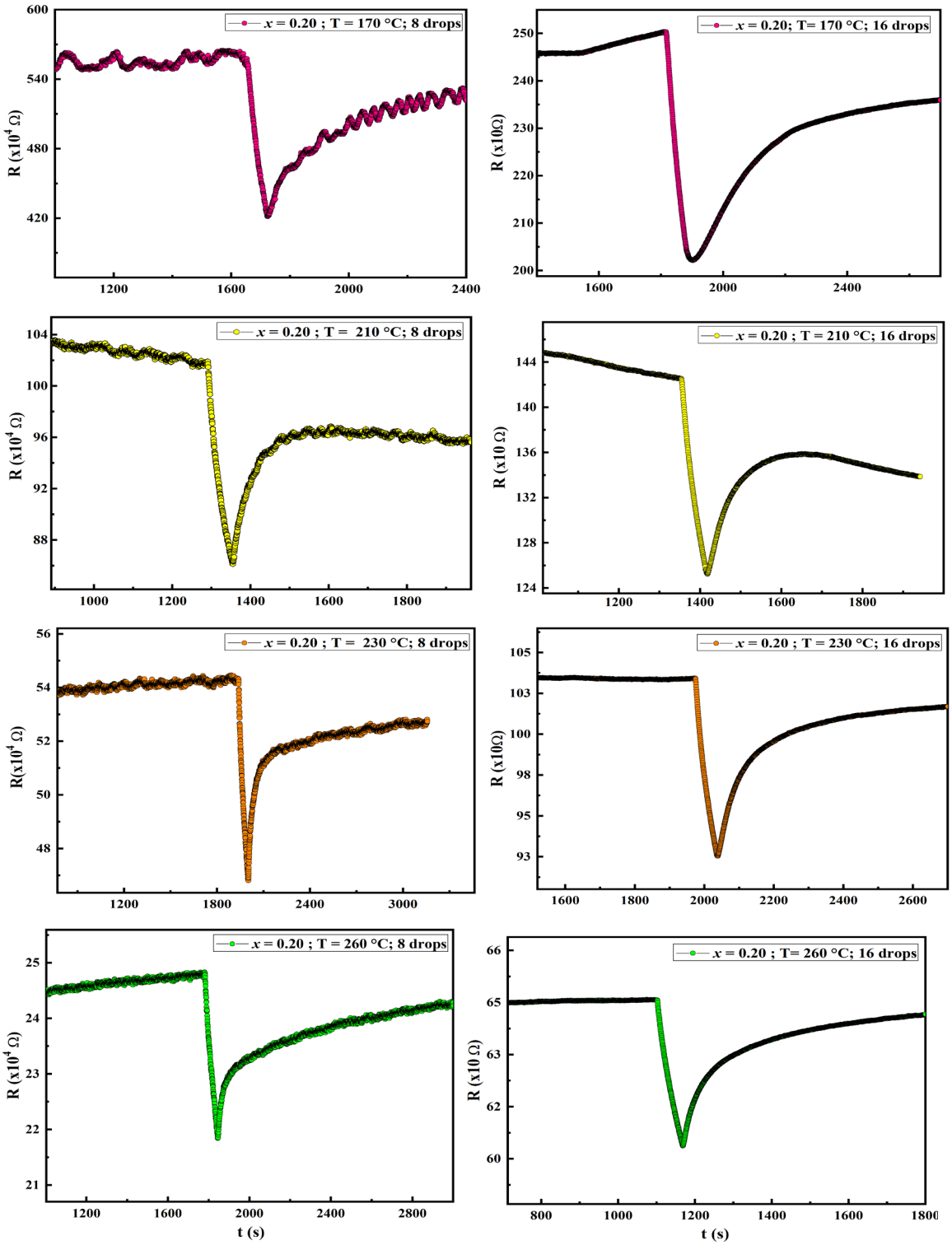

Figure 6: Ozone gas response of $La_{0.8}Pb_{0.1}Ca_{0.1}Fe_{0.8}Co_{0.2}O_3$ ($x = 0.20$) sensor as a function of time at several temperatures ($170, 210, 230$ and $260\ °C$) for a thickness film equal to $300\ nm$ (8 drops) and $600\ nm$ (16 drops) for an exposure time equal to $1\ min$ ($C = 100\ ppb$).

Furthermore, the response (S) of $La_{0.8}Pb_{0.1}Ca_{0.1}Fe_{1-x}Co_xO_3$ (x = 0.10 and x = 0.20) sensors for thickness films equal to 300 nm and 600 nm for an exposure time equal to 1min has been performed. The decrease of the resistance when sensors are exposed to O_3 gas, which is an oxidizing gas, indicates the p-type semiconductor behaviour of the studied sensors **[39]**. The responses obtained with the thickness 300 nm are higher than those found with a thickness of 600 nm. In fact, when the thickness of the film increases, the electrodes are buried **[40]**. Then, the oxygen species are trapped at the top of the $La_{0.8}Pb_{0.1}Ca_{0.1}Fe_{1-x}Co_xO_3$ (x = 0.10 and x = 0.20) film, which reduces the diffusion in the part between the electrodes, inducing the response decrease. On the other hand, the result show that for $x = 0.10$ and at $T = 210$, 230 and 260 °C, the $R(t)$ curve does not return to the baseline. This variation depends on the amount of oxygen adsorbed on the surface because the electron trapped by the oxygen at the surface from the semiconductor decreases the resistance by increasing the major charge carrier ($hole$) concentration **[39]**. However, for a temperature equal to 190 °C, we observe the presence of some stability of $R(t)$ curve. So, we can predict that the operating temperature is expected to be equal to 190 °C for $x = 0.10$ sensor and this temperature decreases to 170 °C for $La_{0.8}Pb_{0.1}Ca_{0.1}Fe_{0.8}Co_{0.2}O_3$ sensor.

Figure. 7 summarizes the ozone response (S) values of $La_{0.8}Pb_{0.1}Ca_{0.1}Fe_{1-x}Co_xO_3$ (x = 0.10 and x = 0.20) with a thickness film equal to 300 nm and 600 nm per each sensor in presence of O_3 gas when concentration is equal to 100 ppb at different working temperatures. As it is known, each sensor can be characterized by its optimal operating temperature (T_O) because the temperature has a significant effect on the gas response.

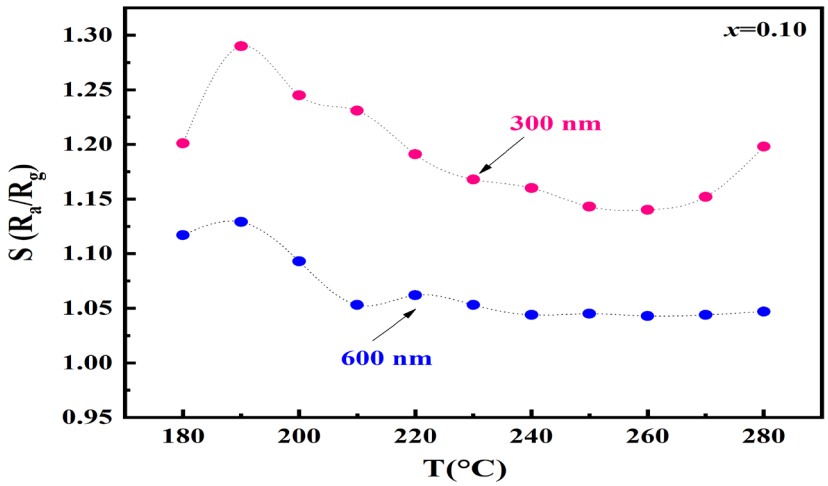

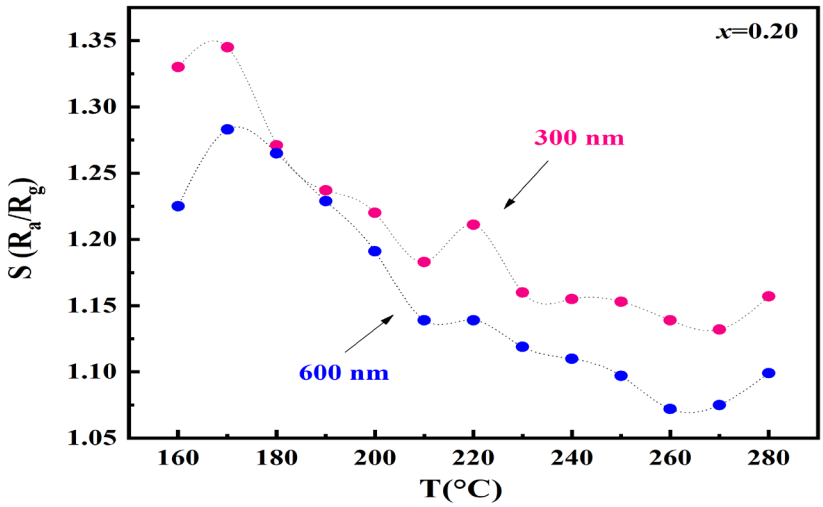

Figure 7: The relationship between response $(S = R_a/R_g)$ and temperature (T) of $La_{0.8}Pb_{0.1}Ca_{0.1}Fe_{1-x}Co_xO_3$ (x = 0.10 and x = 0.20) based sensor during ozone exposing time of 1 min at 100 ppb concentration as a function of film thickness.

***Figure*. 7** reveals that the optimum operating temperatures (T_O) for our sensors was found to be equal to 190 $°C$ and 170 $°C$ for $x = 0.10$ and 0.20, respectively. Lee and reedy **[41]** have revealed that many factors, such as oxygen species, the rates of adsorption and desorption, and the charge carrier concentration, contribute to the sensor response. The activities of the electrons and oxygen species in the sensing reactions depend on the operating temperatures **[42].**

From ***Figure* 5**, we can note that the S values increase not only by decreasing film-thickness, but also by increasing cobalt rate **[43]**.

To further investigate the attitude of $La_{0.8}Pb_{0.1}Ca_{0.1}Fe_{1-x}Co_xO_3$ (x = 0.10 and x = 0.20) sensors to detect various ozone concentrations levels, the sensitivity of the prepared sensors in presence of different concentration of ozone gas for an exposure time equal to 4 min were investigated and the results are shown in ***Figure* 8** ($x = 0.10$) and ***Figure* 9** ($x = 0.20$). The results show that curves present partial reversibility to the base line of $La_{0.8}Pb_{0.1}Ca_{0.1}Fe_{1-x}Co_xO_3$ (x = 0.10 and x = 0.20) sensors towards 50, 100, 200, 300, and 400 ppb at the operating temperature.

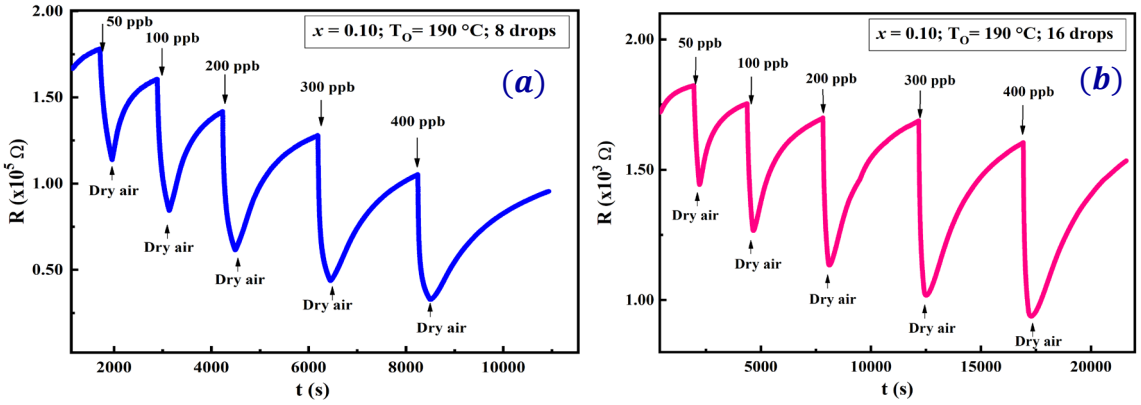

Figure 8: $La_{0.8}Pb_{0.1}Ca_{0.1}Fe_{0.9}Co_{0.1}O_3$ ($x = 0.10$) sensor response (S) to different oxidizing gas (O_3) concentrations ($50, 100, 200, 300\ and\ 400\ ppb$) for a film thickness equal to 300 nm (8 drops) and 600 nm (16 drops) at $T_O = 190\ °C$ and for an exposure time equal to 4 min.

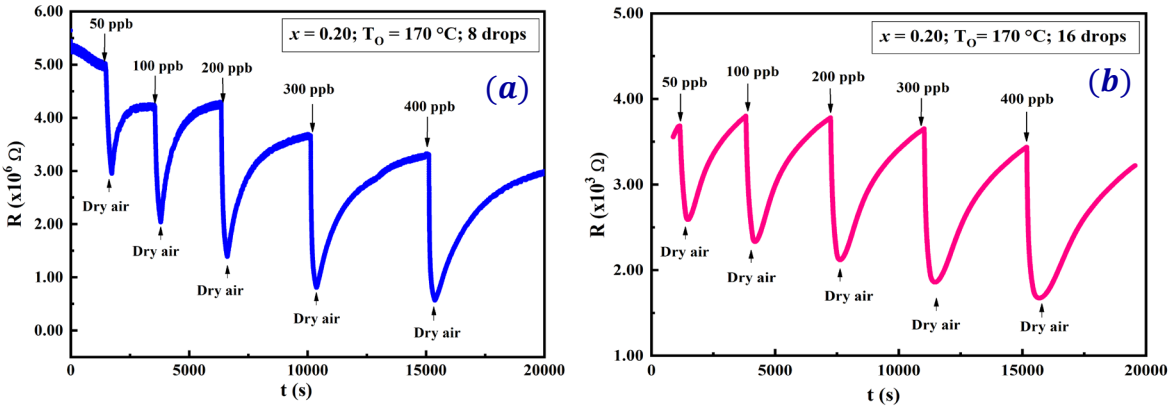

Figure 9: $La_{0.8}Pb_{0.1}Ca_{0.1}Fe_{0.8}Co_{0.2}O_3$ ($x = 0.20$) sensor response (S) to different oxidizing gas (O_3) concentrations ($50, 100, 200, 300$ and $400\ ppb$) for a film thickness equal to 300 nm (8 drops) and 600 nm (16 drops) at $T_O = 170\ °C$ and for an exposure time equal to 4 min.

All characteristics of gas sensors, such as signal, response, and recovery times, depend on the gas diffusion effects and the rate of reaction. This phenomenon is demonstrated theoretically, using the model of SnO_2 **[37]**. When oxygen species are adsorbed, a depletion layer is formed on the surface of the sensing films.

$$O_{2(gas)} \leftrightarrow O_{2(ads)} \qquad (\boldsymbol{Eq.3})$$

$$O_{2(ads)} + e^- \leftrightarrow O^-_{2(ads)} \qquad (\boldsymbol{Eq.4})$$

$$O^-_{2(ads)} + e^- \leftrightarrow 2O^-_{ads} \qquad (\boldsymbol{Eq.5})$$

$$O^-_{(ads)} + e^- \leftrightarrow O^{2-}_{(ads)} \qquad (\boldsymbol{Eq.6})$$

The chemical reactions process between free adsorption site S and the triatomic gases, as ozone (O_3), are Eq.7 and Eq.8 **[44].** These reactions depends also in the operating temperature of each sensor:

$$S + O_3 \rightarrow (S-O) + O_2 \qquad (\boldsymbol{Eq.7})$$

$$(S-O) + e^- \rightarrow (S+O)^- \qquad (\boldsymbol{Eq.8})$$

The response of $La_{0.8}Pb_{0.1}Ca_{0.1}Fe_{1-x}Co_xO_3$ ($x = 0.10$ and $x = 0.20$) detectors increases, simultaneously, by the increases of the gas concentrations and the decreases of film thickness from 300 nm to 600 nm (***Figure* 10** and ***Table* 2**).

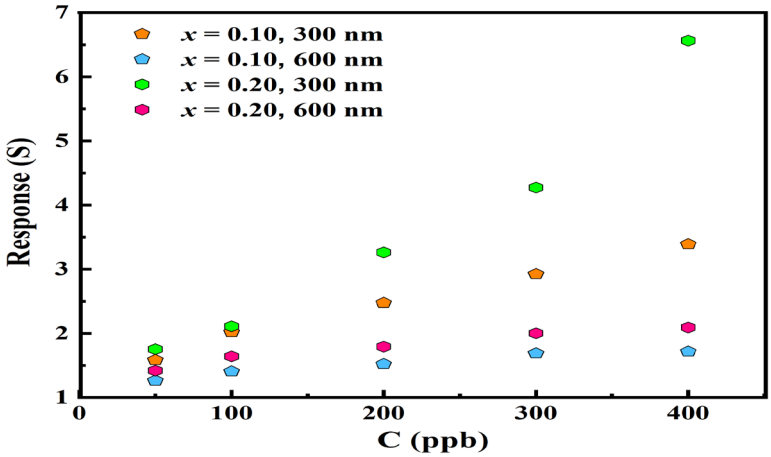

Figure 10: Response ($S = R_a/R_g$) *vs.* O_3 concentrations (50, 100, 200, 300 and 400 ppb) at the working temperature ($T = 190\ °C$) for $x = 0.10$ and ($T = 170\ °C$) for $x = 0.20$ sensors.

Table 2: Response $(S = R_a/R_g)$ of $La_{0.8}Pb_{0.1}Ca_{0.1}Fe_{1-x}Co_xO_3$ ($x = 0.10$ *and* $x = 0.20$) sensors during an ozone exposing time of 4 min at different gas concentrations as a function of film thickness (300 nm and 600 nm).

$C\ (ppm)$	$S\ (0.10)$ 300 nm	$S\ (0.10)$ 600 nm	$S\ (0.20)$ 300 nm	$S\ (0.20)$ 600 nm
0.05	1.586	1.264	1.753	1.420
0.1	2.020	1.407	2.111	1.642
0.2	2.475	1.523	3.264	1.793
0.3	2.926	1.690	4.273	2.001
0.4	3.391	1.716	6.563	2.091

Moreover, the response of the prepared sensors was found higher than the response reported for other metal oxide semiconductor (***Table. 3***) **[45-47]**, and than other perovskite materials cited as potentials O_3 sensing **[48]**.

Table 3: Comparison of sensing performances of different sensors for the detection of O_3.

Sensors	T_O (°C)	$C(ppm)$	Response (S)	Ref
SnO_2	20	0.217	1.6	[45]
CuO	250	0.6	2.5	[46]
$Zn-MoS_2$	25	5	1.8	[47]
$SmFe_{0.8}Co_{0.2}O_3$	200	400	3	[48]

The response and recovery times have been investigated, and the results have been illustrated in ***Table 4***.

Table 4: Response (τ_{resp}) and recovery (τ_{rec}) times of $La_{0.8}Pb_{0.1}Ca_{0.1}Fe_{1-x}Co_xO_3$ (x = 0.10 and x = 0.20) sensors for a thicknesses film equal to 300 nm and 600 nm at different concentrations (C) at the operating temperature for each sensor.

Sensors	T (°C)	C (ppb)	τ_{resp} (min)	τ_{rec} (min)
$x = 0.10$: 300 nm	190	50	3.3	10.2
		200	2.2	21.2
		400	1.9	30.1
$x = 0.10$: 600 nm	190	50	3.5	26.1
		200	3.3	49.9
		400	3.1	58.3
$x = 0.20$: 300 nm	170	50	3.5	8.3
		200	2.5	14.1
		400	2.1	41.3
$x = 0.20$: 600 nm	170	50	2.8	28.2
		200	2.6	44.6
		400	2.3	52.4

The response time is the time needed to reach 90% of the final steady state signal and the recovery time (return time) was defined as the time needed to reach 10% of the final

steady state signal **[49]**. In the case of our sensors, the response time (τ_{resp}) increases from 1.95 min to 3.12 min for $x = 0.10$ when concentration is equal to 400 ppb and when thickness film increases from 300 nm to 600 nm.

IV-CONCLUSION

The present work demonstrates the feasibility of the use of $La_{0.8}Pb_{0.1}Ca_{0.1}Fe_{1-x}Co_xO_3$ (x = 0.10 and x = 0.20) films deposited by drop coating, as ozone sensors.

$La_{0.8}Pb_{0.1}Ca_{0.1}Fe_{1-x}Co_xO_3$ (x = 0.10 and x = 0.20) structural properties revealed the presence of an orthorhombic structure with nanometric grain size. The study of the response $(S = R_g/R_a)$ of our compounds proves the ability of our samples to detect low concentration equal to 50 ppb $(sub - ppm)$ of ozone gas. Responses are more important in case of a thickness film equal to 300 nm compared to those found in case of film thickness of 600 nm. The optimal working temperature was found to be equal to 190 °C with $x =$ 0.10 and decreases to 170 °C for the sample doped with 20% of cobalt.

References

[1] L. Yu, Y. Li, H. Yu, K. Zhang, X. Wang, X. Chen, J. Yue, T. Huo, H. Ge, K. Alamry, H. Marwani and S. Wang, A fluorescence probe for highly selective and sensitive detection of gaseous ozone based on excited-state intramolecular proton transfer mechanism, J. Sens. Actuat. B Chem, 266 (2018) 717.

[2] Risk and Benefits Group, Health Risk and Exposure Assessment for Ozone, book, 2014.

[3] D. Zhang, Z. Yang, P. Li and X. Zhou, Ozone gas sensing properties of metal-organic frameworks-derived In_2O_3 hollow microtubes decorated with ZnO nanoparticles, J. Sens. Actuat. B Chem, 301 (2019) 127081.

[4] A. Catto, L. Silva, C. Ribeiro, S. Bernardini, K. Aguir, E. Longo and V. Mastelaroa, An easy method of preparing ozone gas sensors based on ZnO nanorods, J. RSC Adv. 5 (2015) 19528.

[5] B. Liu, S. Wang, Z. Yuan, Z. Duan, Q. Zhao, Y. Zhang, Y. Su, Y. Jiang, G. Xie and H. Tai, Novel chitosan/ZnO bilayer film with enhanced humidity-tolerant property: Endowing triboelectric nanogenerator with acetone analysis capability, Nano energy, 78 (2020) 105256.

[6] J. Huang, X. Wang, Y. Gong, Y. Liu, P. Zhou, X. Suo, D. Zeng and H. Li, Construction of WO_3coatings with micro-nano hybrid structures by liquid precursor flame spray for enhanced sensing performances to sub-ppm ozone, J. Mater. Lett. 205 (2017) 106.

[7] M. Bendahan, J. Guerin, R. Boulmani, K. Aguir, WO3 sensor response according to operating temperature: Experiment and modelling, J. Sens. Actuat. B Chem, 124 (2007) 24– 29.

[8] C. Jeng, P. Chong, C. Chiu, G. Jiang, H. Lin, R. Wu and C. Wu, A dynamic equilibrium method for the SnO_2-based ozone sensors using UV-LED continuous irradiation, J. Sens. Actuat. B Chem, 195 (2014) 702.

[9] D. Klaus, D. Klawinski, S. Amrehn, M. Tiemann and T. Wagner, Light-activated resistive ozone sensing at room temperature utilizing nanoporous In_2O_3 particles: influence of particle size, J. Sens. Actuat. B Chem, 217 (2015) 181.

[10] S. Bano, A.S. Ganie, S. Sultana, M.Z. Khan and S. Sabir, The non-enzymatic electrochemical detection of glucose and ammonia using ternary biopolymer based-nanocomposites, New. J. Chem, 2021.

[11] O. Yang, L. Zhou, L. Peng, G. Yuan, H. Ding, L. Tan and Y. Zhou, A smart mitochondria-targeting TP-NIR fluorescent probe for the selective and sensitive of H2S in living cells and mice, $New. J. Chem$, 2021.

[12] V. Adepu, N. Bokka, V. Mattela and P. Sahatiya, A highly electropositive ReS2 based ultra-sensitive flexible humidity sensor for multifunctional applications, New. J. Chem, 45 (2021) 5855 − 5862.

[13] M.R. Sovizi and S. Mirzakhani, A chemiresistor sensor modified with lanthanum oxide nanoparticles as a highly sensitive and selective sensor for dimethylamine at room temperature, New. J. Chem, 44 (2020) 4927 − 4934.

[14] K. Aguir, S. Bernardini, B. Lawson and T. Fiorido, Trends in metal oxide thin films: Synthesis and applications of tin oxide, Tin Oxide Materials, (2020)219-246.

[15] W. Avansi Jr, A.C. Catto, L.F. da Silva, T. Fiorido, S. Bernardini, V.R. Mastelaro, K. Aguir and R. Arenal, One-dimensional V_2O_5/TiO_2 heterostructures for chemiresistive ozone sensors, ACS Appl. Nano Mater. 2 (2019) 4756–4764.

[16] L. F. d. Silva, A. C. Catto, S. Bernardini, T. Fiorido, J.V. N. de Palma, W. Avansi Jr, K. Aguir and M. Bendahan, BTEX gas sensor based on hematite microrhombuses, J. Sens. Actuat. B Chem, 326 (2021) 128817.

[17] A. Shahmoradi, A. Hosseini, A. Akbarinejad and N. Alizadeh, Noninvasive Detection of Ammonia in the Breath of Hemodialysis Patients Using a Highly Sensitive Ammonia Sensor Based on a Polypyrrole/Sulfonated Graphene Nanocomposite, American Chemical Society, 2021.

[18] R. Souissi, N. Bouguila, M. Bendahan, T. Fiorido, K. Aguir, M. Kraini, C. Vázquez and A. Labidi, Highly sensitive nitrogen dioxide gas sensors based on sprayed β-In2S3 film, J. Sens. Actuat. B Chem, 319 (2020) 128280.

[19] L.F.d. Silva, V.R. Mastelaro, A.C. Catto, C.A. Escanhoela, J.S. Bernardini, S.C. Zílio, E. Longo and K. Aguir, Ozone and nitrogen dioxide gas sensor based on a nanostructured $SrTi_{0.85}Fe_{0.15}O_3$thin film, J. Alloys. Compds, 638 (2015) 374.

[20] M. Mori, J. Fujita, Y.I. tagaki and Y. Sadaoka, Ozone detection in air using $SmFeO_3$ gas sensor for air quality classification, J. Cera. Soc. Japan, 119 (2011) 926.

[21] V.R. Mastelaro, S.C. Zilio, L.F.D. Silva, P.I. Pelissari, M.I.B. Bernardi, J. Guerin and K. Aguir, Ozone gas sensor based on nanocrystalline $SrTi_{1-x}Fe_xO_3$ thin films, J. Sens. Actuat. B Chem, 181 (2013) 919.

[22] G. Kang, Z. Zhu, B.H. Tang, C.H. Wuand and R.J. Wu, Rapid detection of ozone in the parts per billion range using a novel Ni–Al layered double hydroxide, J. Sens. Actuat. B Chem, 241 (2017) 1203.

[23] Y. Itagaki, M. Mori, Y. Hosoya, H. Aono and Y. Sadaoka, O_3 and NO_2 sensing properties of $SmFe_{1-x}Co_xO_3$ perovskite oxides, J. Sens. Actuat. B Chem, 122 (2007) 315.

[24] W. Belkacem, A. Labidi, J. Guerin, N. Mliki and K. Aguir, Cobalt nanograins effect on the ozone detection by WO3 sensors, J. Sens. Actuat. B Chem, 132 (2008) 196– 201.

[25] S. Thirumalairajan, K. Girija, V.R. Mastelaro and N. Ponpandian, Surface morphology-dependent room-temperature $LaFeO_3$ nanostructure thin films as selective NO_2 gas sensor prepared by radio frequency magnetronsputtering, J. ACS Appl. Mater. Interfaces 6 (2014) 13917.

[26] S. Palimar, S.D. Kaushik, V. Siruguri, D. Swain, A.E. Viegas, C. Narayana and N.G. Sundaram, Investigation of Ca substitution on the gas sensing potentiel of $LaFeO_3$ nanoparticles towards low concentration NO_2 gas, J. Dalton Trans, 45(2016) 13547.

[27] Y. Zhang, Z. Duan, H. Zou and M. Ma, Fabrication of electrospun $LaFeO_3$ nanotubes via annealing technique for fast ethanol detection, J. Mater. Sci. Lett, 215 (2018) 58 − 61.

[28] J. Mizusaki, M. Ynshihiro, S. Yamauchi and K. Fueki, Non stoichiometry and defect Structure of the perovskite-type oxides $La_{1-x}Sr_xFeO_{3-\delta}$, J. Solid State Chem., 58 (1985) 257 − 266.

[29] S. Smiy, H. Saoudi, A. Benali, M. Bejar, E. Dhahri, T. Fiorido, M. Bendahan and K. Aguir, Correlation between structural, magnetic and gas sensor properties of $La_{0.885}Pb_{0.005}Ca_{0.11}Fe_{1-x}Co_xO_3$ compounds, J. Mater. Res. Bull, 130 (2020) 110922.

[30] J. Mizusaki, M. Yoshihiro, S. Yamauchi and K. Fueki, Thermodynamic quantities and defect equilibrium in the perovskite-type oxide solid solution $La_{1-x}FeO_{3-\delta}$, J. Solid State Chem, 67 (1987) 1 − 8.

[31] L.B. Kong, Y.S. Shen, Gas-sensing property and mechanism of $Ca_xLa_{1-x}FeO_3$ ceramics, Sensors and Actuators B, 30 (1996) 217 − 221.

[32] P. Song, H. Qin, L. Zhang, K. An, Z. Lin, J. Hu, M. Jiang, The structure, electrical and ethanol-sensing properties of $La_{1-x}Pb_xFeO_3$ perovskite ceramics with $x \leq$ 0.3, Sensors and Actuators B, 104 (2005) 312 − 316.

[33] H.Y. Li, C.S. Lee, D. H. Kim and J.H. Lee, Flexible Room-Temperature NH3 Sensor for Ultrasensitive, Selective, and Humidity-Independent Gas Detection, J. ACS Appl. Mater. Interfaces, 10 (2018) 27858–27867.

[34] J. Mizusaki, M. Yoshihiro, S. Yamauchi, K. Fueki, Thermodynamic quantities and defect equilibrium in the perovskite-type oxide solid solution $La_{1-x}FeO_{3-\delta}$, J. Solid State Chem., 67 (1987) 1 − 8.

[35] A. Benali, M. Bejar, E. Dhahri, M. Sajieddine, M.P.F. Graça and M.A. Valente, Magnetic, Raman and Mossbauer properties of double-doping $LaFeO_3$ perovskite oxides, J. Mat. Chem. Phys. 149-150 (2015) 467.

[36] T. Addabbo, F. Bertocci, A. Fort, M. Gregorkiewitz, M. Mugnaini, R. Spinicci and V. Vignoli, Gas sensing properties and modeling of $YCoO_3$-based perovskite, J. Sens. Actuat. B Chem, 221 (2015) 1137.

[37] S. Smiy, H. Saoudi, A. Benali, M. Bejar, E. Dhahri, T. Fiorido and K. Aguir, New perovskite compound $La_{0.885}Pb_{0.005}Ca_{0.11}FeO_{2.95}$ for gas sensing application, J. Chem. Phys. Lett, 735 (2019) 136765.

[38] S. Vallejos, V. Khatko, J. Calderer, I. Gracia, C. Cané, E. Llobet and X. Correig, Micro-macined WO_3-based sensors selective to oxidizing gases, J. Sens. Actuat. B Chem, 132 (2008) 209.

[39] A. Bejaoui, J. Guerin, J.A. Zapien and K. Aguir, Theoretical and experimental study of the response of CuO gas sensor under ozone, J. Sens. Actuat. B Chem, 190 (2014) 8.

[40] H.Y. Li, C. S. Lee, D. H. Kim and J.H. Lee, Flexible Room-Temperature NH_3 Sensor for Ultrasensitive, Selective, and Humidity-Independent Gas Detection, ACS Appl. Mater. Interfaces, 10 (2018) 27858 − 27867.

[41] A.P. Lee and B. Reedy, Temperature modulation in semiconductor gas sensing, J. Sens. Actuat. B Chem, 60 (1999) 35.

[42] Z. Gergintschew, H. Forster, J. Kositza, D. Schipanski, Two-dimensional numerical simulation of semiconductor gas sensors, J. Sens. Actuat. B Chem, 26 (1995) 170.

[43] T. Elavarasan, S. Ernest and S. Fairose, Influence of cobalt doping on the structural, optical, topographical and sensing properties of spray deposited zinc oxide thin films, Materials Today: Proceedings, (2020).

[44] J. Guerin, M. Bendahan and K. Aguir, A dynamic response model for the WO_3-based ozone sensors, J. Sens. Actuat. B Chem, 128 (2008) 462.

[45] A. Gaddari, F. Berger, M. Amjoud, J.B. Sanchez, M. Lahcini, B. Rhouta, D. Mezzane, C. Mavon, E. Beche and V. Flaud, A novel way for the synthesis of tin dioxide sol–gel derived thin films: application to O_3 detection at ambient temperature, J. Sens. Actuat. B Chem, 176 (2013) 811.

[46] A. Bejaoui, J. Guerin, J.A. Zapien and K. Aguir, Theoretical and experimental study of the response of CuO gas sensor under ozone, Sensors and Actuators B, 190 (2014) 8.

[47] L. Shoa, Z. Wu, H. Duan and T. Shaymurat, Discriminative and rapid detection of ozone realized by sensor array of Zn^{2+} doping tailored MoS_2 ultrathin nanosheets, J. Sens. Actuat. B Chem, 258 (2018) 937.

[48] M. Mori, Y. Itagaki and Y. Sadaoka, Effect of VOC on ozone detection using semiconducting sensor with $SmFe_{1-x}Co_xO_3$ perovskite-type oxides, J. Sens. Actuat. B Chem, 163 (2012) 44.

[49] R. Waser, Nanoelectronics and Information Technology: Advanced Electronic Materials and Novel Devices, Wiley-VCH, Weinheim, Germany (2005).